Reconstructing environments of collection sites from archaeological bivalve shells: Case study from oysters (Lyon, France)

Vincent Mouchi, Justine Briard, Stéphane Gaillot, Thierry Argant, Vianney Forest, Laurent Emmanuel

1   Reconstructing environments of collection sites from archaeological bivalve shells: case

2   study from oysters (Lyon, France)

3

4   Vincent Mouchi[1]*, Justine Briard[1], Stéphane Gaillot[2], Thierry Argant[3,4], Vianney Forest[5],

5   Laurent Emmanuel[1]

6

7   [1]: Sorbonne Universités, UPMC-Univ. Paris 06, CNRS UMR 7193, Institut des Sciences de la

8   Terre de Paris (ISTeP), case 116, 4 pl. Jussieu, 75005 Paris, France

9   [2]: Service archéologique de la ville de Lyon, 10 rue Neyret, FR-69001 Lyon

10   [3]: Éveha, Études et valorisation archéologiques, agence Rhône-Alpes, 87 avenue des

11   Bruyères – 69150 Décines-Charpieu, France

12   [4]: Laboratoire Archéométrie et Archéologie - UMR 5138

13   [5]: INRAP-Méditerranée, TRACES-UMR5068-Toulouse, France

14   *: Corresponding author, current address: vmouchi@gmail.com

15

16

17   **Abstract**

18   The flat oyster, *Ostrea edulis*, was consumed as a luxury dish by the Romans in antiquity.

19   Numerous shells are found in archaeological sites in the Lyon region, Central France. This

20   area is located over 250 kilometres away from the nearest coastline (the Mediterranean Sea)

21   and little is known about the origin of these oysters prior to transport for consumption. The

22   chemistry of biogenic carbonates reflects that of the fluid they precipitate from at the time

23   of formation. Stable isotopes and Mg/Ca ratios in oyster shells have previously been used as

24   palaeoenvironmental proxies. As Mg/Ca ratio amplitude in bivalve shells has been reported

25 to differ according to local hydrologic settings, we suggest that geochemical differences

26 observed in each shell can be used to identify the type of environment (e.g. estuary, lagoon

27 or marine) from which the specimens originated.

28 In this study, we analyzed the elemental composition of six archaeological *O. edulis* shells of

29 unknown provenance, collected in the Lyon region dated from the 3rd century AD to the 5th

30 century AD. In addition, stable carbon and oxygen analyses from three of these specimens

31 were performed to reconstruct intra-annual fluctuations of seawater chemistry. Overall

32 results show a strong heterogeneity in values. One shell exhibits large fluctuations in δ^{13}C

33 (from -2 to 1 ‰) and δ^{18}O (from -2 to 3 ‰), interpreted as evidence for an estuarine origin.

34 The Mg/Ca amplitude (from 5 to 35 mmol.mol^{-1}) also indicates proximity to a river outlet, as

35 such values were previously reported from modern estuarine oyster shells. Two other

36 specimens present a restricted amplitude in Mg/Ca values (from ~0 to 5 mmol.mol^{-1}), similar

37 to values measured in modern open marine locations. Four other specimens exhibited

38 intermediate Mg/Ca ratios and more restricted stable isotope composition ranges which

39 indicate that these specimens lived in waters with limited freshwater input.

40 The geochemical data from these shells support the hypothesis that fishermen of Antiquity

41 collected oysters from a variety of environments/locations. A clear identification of the living

42 localities of these specimens is still to be defined, as the present data cannot discriminate

43 whether these shells originated from the Mediterranean Sea or the Atlantic Ocean coastline.

44

45

46 **Introduction**

47 The flat oyster, *Ostrea edulis*, was consumed as a luxury dish by the Romans during

48 Antiquity. As a result, numerous shells are commonly found in archaeological sites of rich

49   dwelling places in the Lyon region, Central France. As this city is 250 km away from the

50   nearest coastline (Mediterranean Sea), these specimens were transported for consumption

51   and little is known on their locality of origin during the Roman Empire. Bardot-Cambot

52   (2014) reconstructed a map of commercial routes from this period, and suggested that most

53   molluscs in Lyon originated from the Mediterranean Sea. Though still debated, oyster

54   farming on the French Mediterranean coastline is thought to have started during the 19th

55   century AD (Bardot-Combot and Forest, 2013; Faget, 2007). Using an archaeozoological

56   approach applied to Roman shells supplemented by written sources analysis, Bardot-Combot

57   and Forest (2013) suggested that Romans did not perform aquaculture *per se* and probably

58   collected wild oysters. Hence, the exact localities and living environments of fished oysters

59   remain unknown.

60   The environmental record of geochemical fluctuations in oyster shells represents a

61   promising proxy for palaeoenvironment reconstructions. Oysters appeared over 200 million

62   years ago and their thick calcite shells are generally preserved with regards to diagenesis

63   (Stenzel, 1971). Moreover, they offer sufficiently large structures for high-resolution

64   sampling to study intra-annual (e.g. seasonal) fluctuations for several consecutive years of

65   growth (Kirby et al., 1998; Lartaud et al., 2010a; Surge and Lohmann, 2008).

66   The chemistry of biogenic carbonates reflects that of the fluid it precipitates from at the time

67   of formation (Epstein et al., 1951, 1953; McCrea, 1950). Bivalve shells present incremental

68   growth that preserve older parts, which allows for a continuous record of the evolution of

69   seawater composition during the organism's lifespan. Such mollusc shells have been used in

70   Earth Sciences since the middle of the 20th century (Urey et al., 1951) for reconstructing

71   physicochemical parameters of seawater. In particular, seasonal temperature

72   reconstructions of seawater have been proposed for geological timescales (i.e., several

73   hundred million years ago) using fossils (Anderson and Arthur, 1983; Craig, 1965; Epstein et

74   al., 1951, 1953). These estimates from shell analysis are based on modern breeding in

75   natural sites or laboratory experiments under controlled conditions that lead to the

76   formulation of mathematical equations linking shell geochemistry and physicochemical

77   parameters of seawater (i.e., temperature, salinity, pH). These models can subsequently be

78   utilized to determine past environmental settings.

79   Stable carbon isotopes (δ^{13}C) in mollusc shells have been reported to depend on the

80   combination of the influence of both dissolved inorganic carbon (DIC) and organic carbon

81   sources from food consumption (Lartaud et al., 2010b; McConnaughey and Gillikin, 2008). It

82   has been demonstrated that δ^{13}C signals from oyster soft tissues (Gaudron et al., 2016) and

83   shells (Walther and Rowley, 2013) differ from purely marine to estuarine environments due

84   to distinct food sources. In particular, shell δ^{13}C can be used jointly with stable oxygen

85   isotope measurements to indicate flooding events (Walther and Rowley, 2013).

86   Several temperature proxies are commonly used on mollusc shells such as stable oxygen

87   isotope ^{18}O/^{16}O ratios (δ^{18}O; Bougeois et al., 2014, 2016; Duprey et al., 2015; Epstein et al.,

88   1951, 1953; Klein et al., 1996; Lartaud et al., 2010c; Surge and Lohmann, 2008; Surge et al.,

89   2001; Vander Putten et al., 2000). Some uncertainties exist since calcium carbonate of the

90   shells δ^{18}O ($\delta^{18}O_c$) is a function of temperature and seawater δ^{18}O ($\delta^{18}O_w$). This last

91   parameter co-varies with salinity, which is often not properly constrained in the past

92   (Rohling, 2000). A variety of calibrations of $\delta^{18}O_w$ from salinity have been published based on

93   different modern marine settings (e.g., Epstein and Mayeda, 1953; Pierre, 1999; Voelker et

94   al., 2015), and a specific model is chosen according to the studied locality. Classically,

95   palaeosalinities are estimated by studying the ecology of the fauna associated with the

96   studied material or by taking modern values in similar settings. Temperatures are

97   reconstructed from these estimations of $\delta^{18}O_w$ and the measured $\delta^{18}O_c$ (McCrea, 1950).

98   Multiple models also exist for this relationship according to the mineralogy and the taxon.

99   For calcitic mollusc shells, such as oyster shells, the calibration provided by Anderson and

100   Arthur (1983) is relevant and widely utilized (Equation 1).

101   <u>Equation 1:</u> $T = 16 - 4.14 (\delta^{18}O_c - \delta^{18}O_w) + 0.13 (\delta^{18}O_c - \delta^{18}O_w)^2$ (Anderson and Arthur,

102   1983)

103   Strontium to calcium and magnesium to calcium ratios have also been exploited as

104   temperature proxies in biogenic carbonates (Bougeois et al., 2014, 2016; Freitas et al., 2008,

105   2012; Klein et al., 1996; Lazareth et al., 2003; Mouchi et al., 2013; Surge and Lohmann, 2008;

106   Ullmann et al., 2013; Vander Putten et al., 2000; Wanamaker et al., 2008). These Me/Ca

107   ratios in carbonates are also commonly considered to fluctuate according to several factors.

108   Mineralogy has an influence and each locality used for model definition has different

109   environmental settings which are reflected in the shell geochemistry.

110   Although these proxies were proven useless in some bivalve species such as clams (Carré et

111   al., 2006; Gillikin et al., 2005; Poulain et al., 2005; Surge and Walker, 2006) or scallops

112   (Lorrain et al., 2005), temperature seems to be the main factor causing fluctuations within a

113   specimen for mussels and oysters (Freitas et al., 2008; Klein et al., 1996; Mouchi et al., 2013;

114   Surge and Lohmann, 2008; Tynan et al., *in press*; Vander Putten et al., 2000). Still, some vital

115   effects (compositional shifts from seawater composition and physicochemical parameter

116   response) may induce at least a certain amount of geochemical variability (Bougeois et al.,

117   2014, 2016; Mouchi et al., 2013; Saenger and Wang, 2014; Schöne and Gillikin, 2013).

118   Magnesium incorporation in single oyster shells presents different calculated

119   thermodependance equations when considering calcification that occurred from autumn to

120   winter (decreasing temperatures) compared to the period from spring to summer

121   (increasing temperatures), probably due to different metabolic response (see Fig. 6 in

122   Mouchi et al., 2013). This metabolic impact prevents the effective use of Mg/Ca for

123   temperature reconstructions for spring and autumn, restricting estimations from this proxy

124   to thermal amplitude between winter and summer. Mouchi et al. (2013) also reported that

125   high-frequency and large amplitude fluctuations in shell Mg/Ca correspond to successive

126   lunar cycles not related to temperature variations.

127   Finally, for the marine and brackish mussel genus *Mytilus*, a clear locality-specificity was

128   noted in Mg incorporation (Freitas et al., 2008; Klein et al., 1996; Vander Putten et al., 2000;

129   Wanamaker et al., 2008). The same observation was made for the *Saccostrea glomerata*

130   oyster species (Tynan et al., *in press*). A model must therefore be carefully chosen to avoid

131   incorrect interpretations.

132   In this study, using isotopic and elemental analyses of the shells, we gather physicochemical

133   evidence to characterize the historically important fishing areas. As geomorphology of the

134   Mediterranean coastline presented strong heterogeneity in Antiquity (Carozza et al., 2010;

135   Dubar, 2003; Raynal et al., 2010; Rescanières, 2002; Rey et al., 2009), these various settings

136   should be reflected in the geochemistry of oyster shell specimens. In particular, using the

137   locality-specificity of Mg/Ca in oyster shells, we attempt to define whether fishermen had

138   clustered sources of oysters or if they collected from a broader variety of environments.

139   **Materials and Methods**

140   <u>Archaeological sites</u>

141   The oyster specimens (*Ostrea edulis*) used in this study were collected from archaeological

142   sites in Lyon, France. The first site, referred to as Antiquaille (Hofmann, *in prep*), corresponds

143   to an abandoned residential area located on the Fourvière hill, at the heart of the *Lugdunum*

144   primitive colony. Eleven oyster specimens were selected from the community found on this

145   site. The stratigraphic unit from which those shells were collected was dated to the 2nd or 3rd

146   century AD by ceramics.

147   A second collection site corresponds to a filling pit dated to the 5th century AD on the 16 rue

148   Bourgelat site (Bertand, 2011). This large pit (3.70 by 5.5 m) included small items (fauna

149   remains, ceramics) and large quantities of broken parts from furnaces and dwelling places.

150   The quality of these broken parts indicates the demolition of wealthy residences. The top of

151   this pit is in direct contact with the modern age levels. A total of 51 oyster shells were

152   recovered from this site as well as some Bourgogne snails (*Helix pomatia*) shells. Twelve

153   oyster specimens were selected from this site.

154   Finally, three shells were selected from the 8-14 rue Gadagne site, in the Old Lyon district.

155   This site is located on the east side of the Saône River at the base of the Fourvière hill. It was

156   built from 50-70 BC, prior to *Lugdunum* foundation. During the Gallo-Roman age, a large

157   building was occupied between the 3rd and the 4th centuries AD.

158   All specimens are considered to have been consumed by a high social level community and

159   must have travelled some considerable distance from a coastline. Although most specimens

160   probably originated from the Mediterranean Sea, bivalve shells from species endemic to the

161   Atlantic coastline have been discovered on site (Bardot-Cambot, 2014). The exact origin of

162   the oysters consumed in Lyon during Antiquity is therefore still unknown.

163   Oyster shells

164   Specimens presenting no visible perforation in the umbo region by lithophagous fauna were

165   manually cleaned from potential epibionts attached on the shell surface using deionized

166   water. Ultrasonic baths were not utilized due to the fragile aspect of our specimens. The

167   umbo region of the left valve was mounted in resin and cut from the rest of the shell using a

168   Buehler Isomet Low Speed Saw (Huntsman Araldite 2020) in order to prevent the fine

169 lamellae inside the umbo from breaking during preparation. Polished thick sections (200-500

170 µm thick) were cut along the maximum growth axis to expose the inner part of the umbo

171 (Fig. 1). This process allows access to a complete and continuous accretionary growth record

172 on a spatially-restricted area (Bougeois et al., 2014, 2016; Kirby et al., 1998; Langlet et al.,

173 2006; Lartaud et al., 2010a; Mouchi et al., 2013; Richardson et al., 1993).
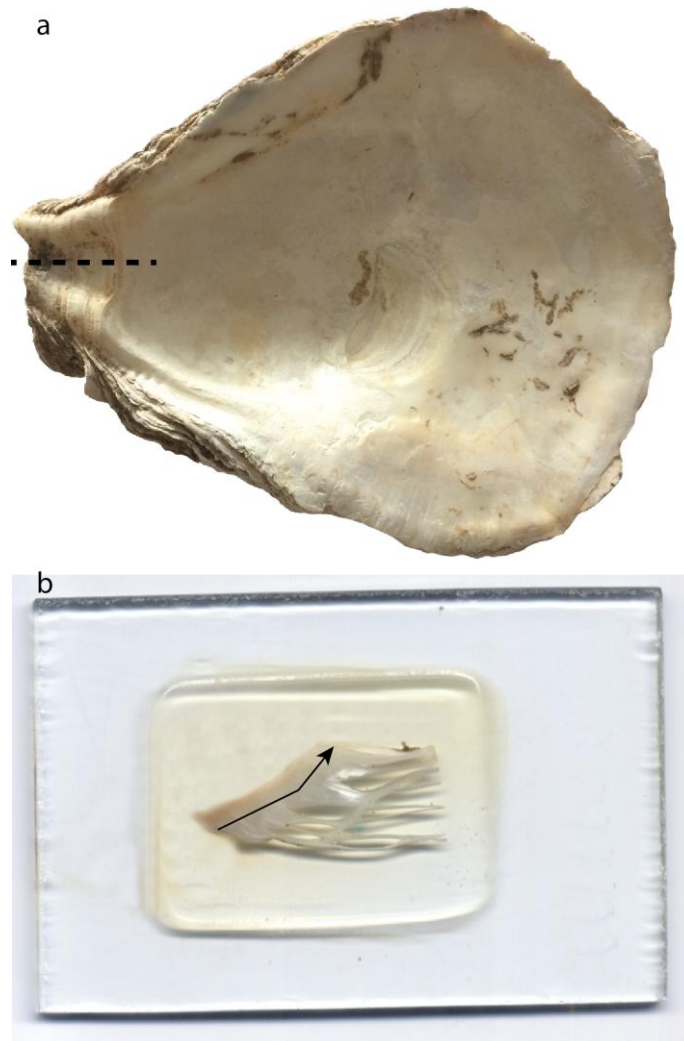

174

175 Figure 1: Oyster sample preparation. a: Left valve of oyster shell showing location and

176 orientation of cut from the umbo. b: Thin section from the cut located on a. The arrow

177 indicates the direction of growth and location of Mg/Ca transect measurements.

178

179 <u>Seasonal calibration using cathodoluminescence</u>

180   The umbo region of each oyster shell was observed under cathodoluminescence (CL) using

181   the principles described in Langlet et al. (2006) and Lartaud et al. (2010c). Natural

182   luminescence is emitted in response to electronic bombardment due to the presence of

183   activators (mainly Mn) within the crystal lattice. The intensity of luminescence (IL) is mainly

184   related to the proportion of Mn^{2+} (de Rafélis et al., 2000). It has been observed that Mn^{2+}

185   incorporation in the shell is increased during summer months compared to the winter

186   (Langlet et al., 2006; Lartaud et al., 2010c). This is due to enhanced phytoplankton

187   consumption in summer (with more frequent blooms), as phytoplankton species can

188   incorporate up to 4 orders of magnitude of Mn compared to surrounding waters (Sunda and

189   Huntsman, 1985). This cyclic annual Mn concentration pattern has been used as a temporal

190   calibration of mineral accretion in the umbo of fossil oyster shells (Bougeois et al., 2014,

191   2016; Lartaud et al., 2006). CL also allows to attest the pristine state of calcium carbonate

192   structures.

193   CL observations were undertaken with a Cathodyne-OPEA cold cathode at 15-20 kV and 200-

194   400 $\mu A.mm^{-2}$, with a pressure of 0.05 Torr. No diagenetic overprint was noted on any of the

195   26 specimens. Assembly of colour pictures of the observation of each specimen was

196   converted to grey-scale and line transects following shell growth in the foliated area were

197   chosen for analysis with the NIH-ImageJ software (v. 1.50i). These transects of grey intensity

198   variations were then used to locate areas of bright luminescence (i.e. are synchronous to

199   summer periods) and dull luminescence (associated to winter periods). Six specimens from

200   the initial 26 were selected for further analyses according to the quality of this temporal

201   calibration: four specimens from stratigraphical units dated to the 2nd or 3rd century AD in

202   Site 1 (US547-1, US654-1, US654-3 and US915-1), one specimen from a stratigraphical unit

203   dated to the 5th century AD in Site 2 (US46-2) and a final specimen from a stratigraphical unit

204   dated to the 4th century AD in site 3 (US118-3).

205   <u>Geochemical analyses</u>

206   *Mg/Ca ratios*

207   The six selected shells were carbon coated and analyzed by electron probe microanalysis

208   (EPMA) at the Camparis service of ISTeP, UPMC, Paris. A CAMECA SX *Five* was used,

209   operating at 25 kV potential with a 130 nA current and 25 µm defocused beam diameter, as

210   used by Mouchi et al. (2013). Detection limits for the measured elements were 100 ppm for

211   Ca and 60 ppm for Mg. A diopside crystal was used as an internal standard for both

212   elements. According to the size of the specimens, successive interconnected transects (to

213   accommodate for the curvature of the umbo; Fig. 1b) were performed along the foliated

214   area of the umbo presenting no obvious physical alteration to obtain several continuous

215   millimeters of elemental measurements per specimen. With the chosen sampling resolution,

216   we obtained between 244 and 497 regularly spaced (25 µm) measurements per shell.

217   High-frequency fluctuations (which do not reflect physicochemical parameters of seawater;

218   Mouchi et al., 2013) were removed by performing a moving average on 15 points on all data

219   series.

220   *Stable oxygen and carbon isotope ratios*

221   Stable carbon and oxygen isotopic analyses were performed on three of the specimens

222   following umbo growth. For each sample, 40 µg of powder were collected from thick

223   sections using a micromill at the Muséum National d'Histoire Naturelle, Paris. Drilling was

224   operated to extract carbonate powder from separated curved transects over 1-2 mm long

225   (depending on the available space of foliated calcite) and 250 µm depth for each sample.

226   Seasonal calibration from CL was used to define a resolution allowing multiple samples per

227   season when possible for consistency over several successive years of accumulation. We

228   collected 12 samples for isotope analysis from specimen US547-1 (2 samples were rejected

229   due to lack of material), 23 samples from specimen US46-2 (no rejection) and 17 samples

230   from specimen US654-1 (1 sample rejected due to lack of material). Carbon dioxide was

231   extracted on carbonate powder using a Kiel IV carbonate device after dissolution in anhydric

232   orthophosphoric acid at 70°C (McCrea, 1950) and analyses were performed on a DELTA V

233   isotope ratio mass spectrometer at the Université Pierre et Marie Curie (Paris, France).

234   Isotope values are reported in delta notation relative to Vienna Peedee Belemnite. Repeated

235   analyses of a marble working standard (calibrated against the international standard NBS-19)

236   indicate an accuracy and precision of 0.1‰ (1 σ).

237   For temperature estimations, the model of Anderson and Arthur (1983; Equation 1) was

238   used for thermodependance of shell $\delta^{18}O$. The model of Pierre (1999), defined from current

239   values of the Mediterranean Sea, was used for estimating $\delta^{18}O_w$ (Equation 2). As a

240   comparative model for $\delta^{18}O_w$, we used the model of Lartaud (2007) which was established

241   from different locations from the French Atlantic and the English Channel coastline

242   (Equation 3).

243   <u>Equation 2:</u> $\delta^{18}O_w = 0.27 * S - 8.9$ Pierre (1999)

244   <u>Equation 3:</u> $\delta^{18}O_w = 0.22 * S - 7.3$ Lartaud (2007)

245

246   **Results**

247   <u>Growth rates</u>

248   According to the studied specimens, different behaviors are observed concerning the growth

249   rates (Fig. 2) when using cathodoluminescence as temporal calibration (high luminescence

250   corresponds to summer periods; low luminescence to winter periods). The specimens US46-

251   2, US654-1, US654-3, US547-1 and US915-1 present a decreasing growth rate over time in

252   accordance to the classic growth model of von Bertalanffy. US915-1 presents very high

253   growth rates during the juvenile stage (> 4 mm.yr^{-1}), whereas shell growth rates from all

254   other specimens range between 1.8 and 3 mm.yr^{-1}. The specimen US118-3 displays a

255   particular behavior with a relatively low juvenile growth rate (1.5 mm.yr^{-1}) and an increase of

256   calcification rate during its fourth and seventh year (based on cathodoluminescence

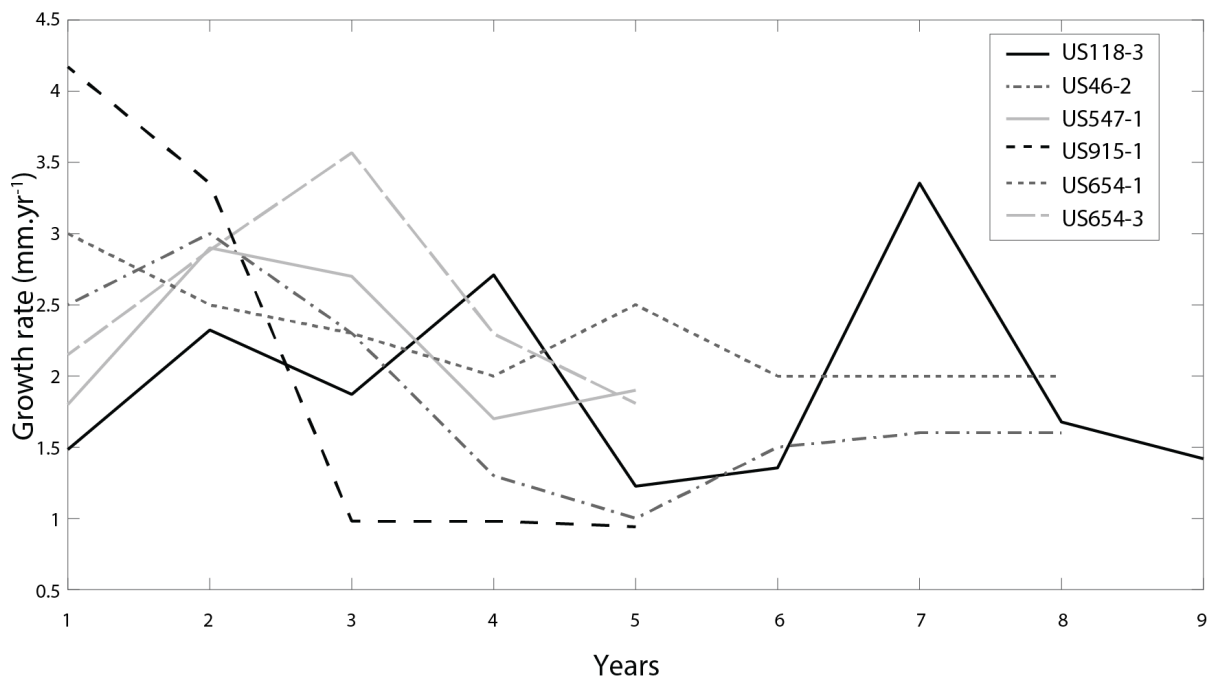257   temporal calibration).

258

259   Figure 2: Reconstructed growth rates from all specimens based on cathodoluminescence

260   temporal calibration (Langlet et al., 2006; Lartaud et al., 2010c).

261

262   <u>Mg/Ca variations</u>

263   All specimens exhibit Mg/Ca fluctuations (Fig. 3). Several groups of specimens can be

264   differentiated from ranges of values of low frequency fluctuations (see smoothed data on

265   Fig. 3). Specimens US547-1 (Fig. 3a) and US654-3 (Fig. 3d) present a range of values from

266   approximately 3 to approximately 10 mmol.mol^{-1}, with mean values of 6.67 ± 2.23 and 5.21

267   ± 3.37 mmol.mol^{-1} for US547-1 and US654-3, respectively. A second group is defined by

268   specimens US118-3 (Fig. 3b) and US915-1 (Fig. 3f) with lower values, generally ranging from

269   approximately 1 to 5 mmol.mol^{-1}, although specimen US118-3 presents increased amplitude

270   with ontogeny. Mean values are 4.90 ± 5.58 and 3.32 ± 2.82 mmol.mol^{-1} for US118-3 and

271   US915-1, respectively. Specimen US654-1 (Fig. 3c) exhibits values ranging from 7 to 12

272   mmol.mol^{-1} approximately (9.99 ± 3.20 mmol.mol^{-1}). Finally, specimen US46-2 (Fig. 3e) has

273   the highest values of the dataset, ranging from 5 to 35 mmol.mol^{-1} with a mean value of

274   19.74 ± 10.70 mmol.mol^{-1}. A positive ontogenic trend is visible for specimen US547-1 (Fig.

275   3a) and a negative trend is visible for specimen U46-2 (Fig. 3e).

276   When compared to luminescence intensity (IL), specimens US118-3 (Fig. 3b), US654-3 (Fig.

277   3d) and US915-1 (Fig. 3f) present a fair graphic correlation between cathodoluminescence

278   signal and Mg/Ca for the entire studied transects. Graphic correlation for specimen US547-1

279   (Fig. 3a) can be validated until 8 mm from the start of the hinge (Fig. 3a). Specimens US547-1

280   and US46-2 exhibit partial graphic correlation only. Specimen US46-2 presents a positive

281   graphic correlation at first from 6 to 8.5 mm on the transect, while the rest of the measured

282   line presents Mg/Ca values that do not reflect any resemblance to the IL signal (Fig. 3e).

283   Relation between these two signals is more complex for specimen US654-1 which seem to

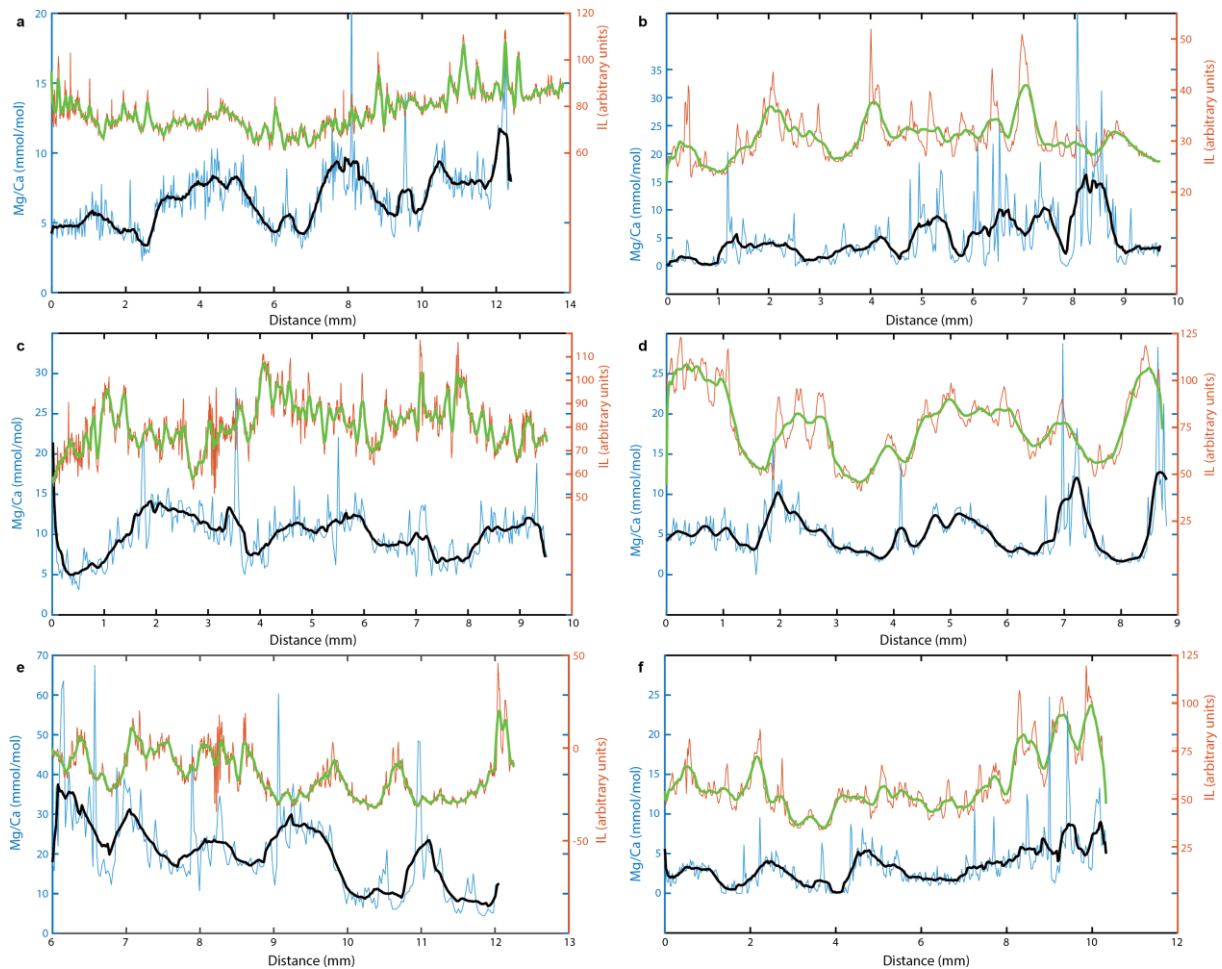284   present a partial anti-correlation from 1 to 4 mm and from 5.5 to 8.5 mm (Fig. 3b).

285

Figure 3: CL intensity of luminescence (IL; in arbitrary units) and Mg/Ca ratio along the
measured transects of all six specimens. The abscissa represents the distance from the start
of the hinge, following growth. Moving average smoothing (15 points for Mg/Ca and 25
points for IL) are also indicated in black (Mg/Ca) and green (IL) for clarity. Note the scales for
Mg/Ca ratios. a: US547-1. b: US118-3. c: US654-1. d: US654-3. e: US46-2 (adult part only). f:
US915-1.

Isotope ratios

The $\delta^{18}O$ values range from -0.50 to 1.68 ‰ (mean: 0.21 ± 0.73 ‰) for specimen US547-1,
from -1.32 to 1.01 ‰ (mean: -0.36 ± 0.67 ‰) for US654-1 and from -1.91 to 2.95 ‰ (mean:
0.54 ± 1.34 ‰) for US46-2 (Fig. 4). The $\delta^{13}C$ values range from 0.53 to 1.48 ‰ (mean: 1.11 ±

297   0.34 ‰), from 0.18 to 0.96 ‰ (mean: 0.56 ± 0.28 ‰) and from -1.66 to 0.80 ‰ (mean: -0.54

298   ± 0.69 ‰) for US547-1, US654-1 and US46-2, respectively.

299   Variations of IL generally present opposed fluctuations with δ^{18}O for specimen US547-1. On

300   the contrary, specimen US654-1 shows synchronous fluctuations of IL and δ^{18}O. Specimen

301   US46-2 presents strong fluctuations with little relation to IL variations.
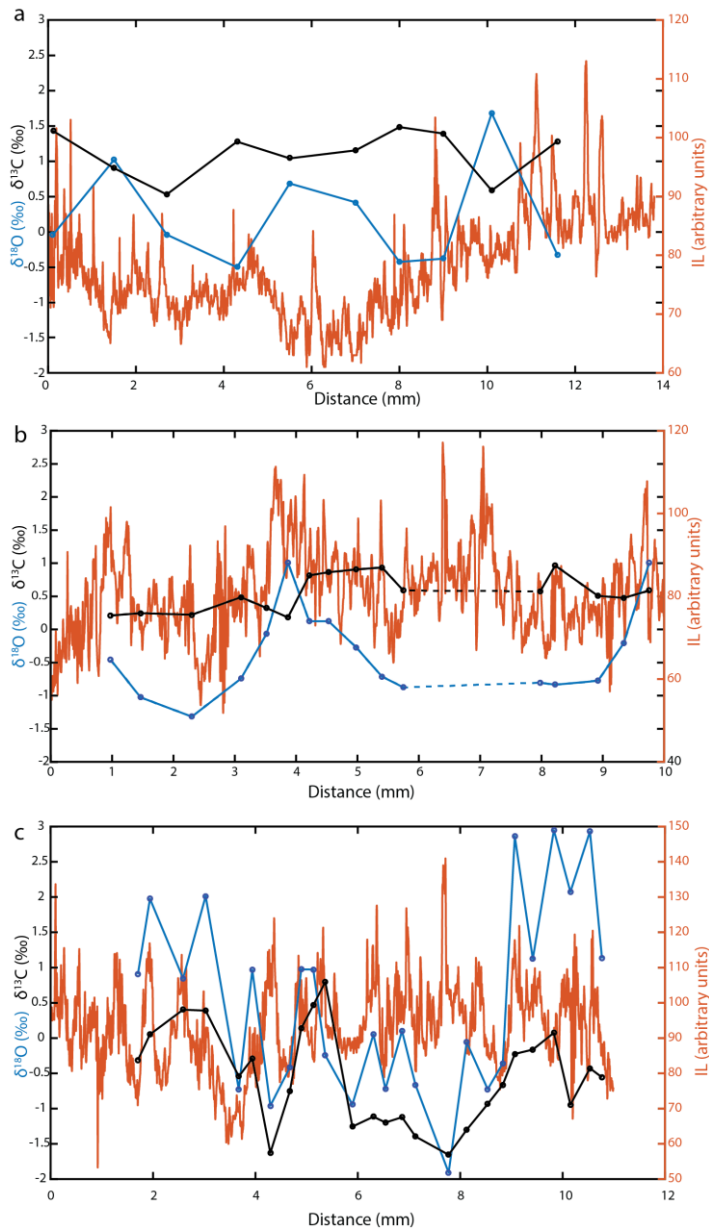

302

303   Figure 4: Isotopic ratios (axis on the left-hand side) from all three shells in relation to CL

304   intensity of luminescence (IL). a: US547-1. b: US654-1. The dashed transect marks a

305   damaged portion of the shell that was not sampled. c: US46-2.

306

Discussion

Reconstructing seasonal evolution of seawater chemistry from stable isotope analyses

When evaluating the results for δ^{13}C and δ^{18}O, additional information can be inferred about

the temporal dynamic change of the surrounding waters along the organism's lifespan.

Figure 5 presents the seasonal record of isotopic composition of the studied shells. Upon

initial observation there is no obvious seasonal difference between δ^{13}C and δ^{18}O for each

specimen (Fig. 5). Secondly, specimens US547-1 and US654-1 are relatively restricted in

amplitude for δ^{13}C, with US547-1 values more enriched than those of US654-1. Finally, US46-

2 presents larger amplitudes in both δ^{13}C and δ^{18}O and δ^{13}C values are generally depleted

compared to the other specimens. In oyster shells, δ^{13}C values generally reflect fluctuations

in dissolved inorganic carbon (DIC) and/or organic carbon from diet (phytoplankton) whose

interactions, challenging to constrain, complicate the interpretation as an environmental

proxy (Emery et al., 2016; Klein et al., 1996; Lartaud et al., 2010b; Surge and Lohmann, 2008;

Surge et al., 2003). Still, this large amplitude indicates that specimen US46-2 was living in a

less stable environment than both other specimens in terms of food supply and salinity.

The initial part of the US46-2 shell presents relatively enriched values for both isotope ratios

(Fig. 4c). Two features are noted for this part of the sequence involving a sudden decrease in

both δ^{13}C and δ^{18}O. A drop in δ^{18}O can be interpreted as both an increase in temperature

and a drop in salinity. If we consider that this specimen originates from the French

Mediterranean coastline, the main river reaching this area is the Rhone River, whose flow is

controlled by the melting of the Alps glaciers. Thus, an increase in temperatures recorded in

the Mediterranean Sea can also be synchronously happening in the Alps and cause stronger

melting, inducing a more pronounced flow of the Rhone River. This larger amount of

330   freshwater, when reaching the shore, would subsequently be responsible for a decrease of

331   salinity, as observed in the present data. However, other possibilities to provide freshwater

332   exist, such as important floods during high-intensity rainfall events. Indeed, it has been

333   reported that strong variations in δ^{13}C and δ^{18}O in oyster shells can be linked to flooding

334   events (Walther and Rowley, 2013). Such events can also be proposed as a cause for a non-

335   seasonal Mn incorporation (and hence CL signal) as nutrient input would vary and induce

336   episodic Mn-rich phytoplankton blooms. Such an interpretation would explain the

337   complexity of the CL signal from this specimen (Fig. 4c) compared to the others.

338   The synchronous decrease in δ^{13}C can also be explained by the same type of event, as cold

339   freshwater reaching the shore from melting glaciers would contain substantial

340   concentrations of nutrients. These nutrients would induce phytoplankton development,

341   reducing the DIC δ^{13}C as organic matter incorporates more ^{12}C, but would provide a

342   substantial food source for the oysters, which would in turn enrich their shells in light

343   carbon.

344   For the rest of the shell, when following growth, several clusters of δ^{13}C and δ^{18}O are

345   recorded. It seems that local seawater conditions lingered at a certain steady-state before

346   being strongly and suddenly changed to a new equilibrium for another few years. Contrary

347   to the other specimens that demonstrate more stable conditions, it seems here that US46-2

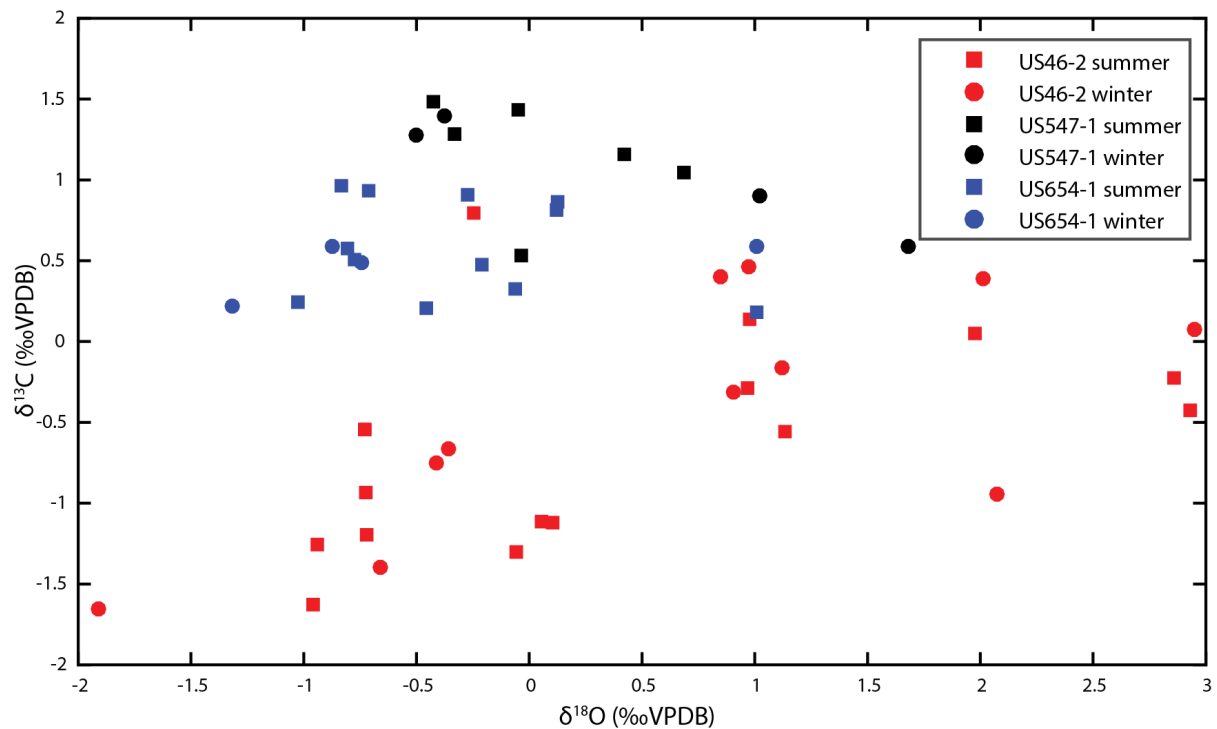348   is native to a dynamic location.

349

350 Figure 5: Isotopic composition of oyster shells. Samples from winter and summer periods of

351 calcification (from interpretation of CL signal) are discriminated. US547-1 (in black, 10

352 samples), US654-1 (in blue, 16 samples) and US46-2 (in red, 26 samples) show 2 different

353 signals. Specimens US547-1 and US654-1 present a restricted amplitude in O and C isotopic

354 composition, while specimen US46-2 exhibits a large amplitude of values for both isotopic

355 ratios.

356

357 <u>Temperature reconstruction using estimated $\delta^{18}O_w$</u>

358 Oxygen isotope ratios were converted to temperatures using the equation of Anderson and

359 Arthur (1983) based on calcitic molluscs (Equation 1). As an estimation of $\delta^{18}O_w$ – required

360 for the temperature calculations – we used the equations of Pierre (1999; Equation 2) and

361 Lartaud (2007; Equation 3), defined from the Mediterranean Sea and the French Atlantic

362 coastline, respectively. To do this, we used a constant modern mean salinity value of 35.5 ‰

363 for the Atlantic area model and 39.0 ‰ for the Mediterranean area model. The

364   corresponding calculated $\delta^{18}O_w$ values from Equations 2 and 3 are 1.63 ‰ and 0.51 ‰ for

365   the Mediterranean Sea and the North-East Atlantic, respectively. Resulting calculations are

366   shown on Figure 6. As growth rates of oyster shells are known to be reduced in winter

367   months (Lartaud et al., 2010c) and since our sampling resolution is spatially constant

368   between consecutive samples, winter values are likely to be overestimated (i.e., samples

369   from winter periods will probably contain parts from previous autumn and/or subsequent

370   spring, inducing an elevated mean value).

371

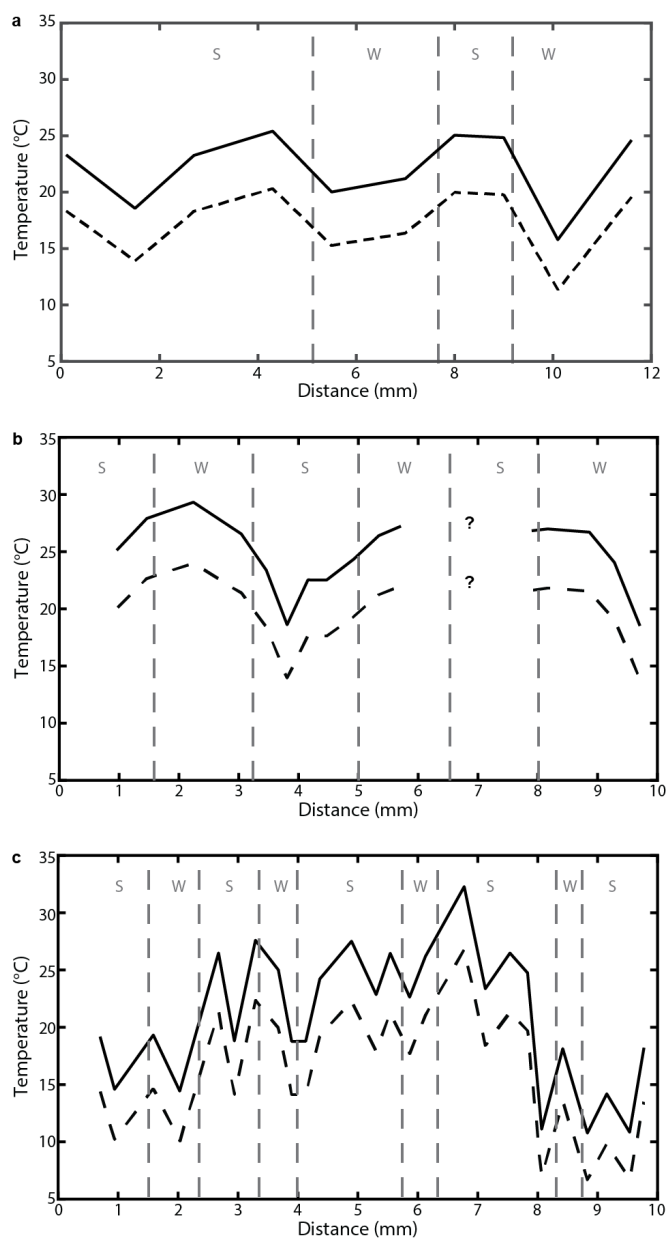372   Figure 6: Temperature reconstruction from $\delta^{18}O$ for two hypothetical origins of the oyster

373   shells: Mediterranean Sea (solid line) and French Atlantic coast (dashed line). Values of $\delta^{18}O_w$

374   used for calculations using the model of Anderson and Arthur (1983) are 1.63 ‰

375   (considering a constant salinity of 39 ‰ and using the model of Pierre, 1999; Equation 2) and

376   0.51 ‰ (considering a constant salinity of 35.5 ‰ and using the model of Lartaud, 2007;

377   Equation 3) for the Mediterranean Sea and the North-East Atlantic, respectively. Limits of

378   winter (W) and summer (S) seasons, based on CL model (Langlet et al., 2006), are located by

379   dashed vertical grey lines. a: US547-1. b: US654-1. The missing transect (underlined by '?'

380   signs) corresponds to a damaged part of the shell that was not sampled. c: US46-2.

381

382   Temperatures reconstructed using this estimated constant $\delta^{18}O_w$ show generally

383   synchronous fluctuations for specimen US547-1 compared to the seasons interpreted from

384   CL signal (Fig. 6a). Temperature values range from 11.3 to 20.3 °C for the Atlantic hypothesis

385   and from 15.8 to 25.4 °C for the Mediterranean Sea hypothesis, though most variations

386   occur over a modelled 6 to 7 °C interval for the entire section, which is lower than the values

387   currently measured on the French coasts (generally 16 °C amplitude for the Mediterranean

388   Sea, from 11 to 27 °C, and approximately 12 °C amplitude for the Atlantic, from 8 to 20 °C;

389   http://www.meteociel.fr/accueil/sst.php). The calculated summer temperature values for

390   the Mediterranean Sea origin hypothesis are in accordance with Luterbacher et al. (2016),

391   who indicated for this period that mean summer temperatures for the studied time period

392   were approximately 2.5°C lower than those from present day.

393   For specimen US654-1, reconstructed temperatures range from 14 to 24 °C for the Atlantic

394   hypothesis, corresponding to a modelled temperature amplitude of 10 °C (Fig. 6b). For the

395   Mediterranean origin hypothesis, reconstructed temperatures range from 18.6 to 29.3 °C.

396   The age model from CL appears here to be contrary to the calculated temperatures. The

397   second winter and third summer indicated by the CL fluctuations has however no

398   corresponding isotope samples to check for this discrepancy. Still, subsequent samples,

399   which would correspond to a winter period, present high temperatures and slowly

400   decreasing at the end of this winter period, which is consistent with previous parts of this

401   shell.

402   Specimen US46-2 presents temperatures ranging from 6.7 to 26.7 °C for the Atlantic

403   hypothesis and from 10.8 to 32.3 °C considering a Mediterranean origin, corresponding to a

404   thermal contrast on the extrema of over 20 °C (Fig. 6c). However, a positive trend is visible

405   from the start to 7.5 mm before a strong drop in values. When comparing to local minima

406   and maxima, the contrast rarely exceeds 10 °C. High and low temperature values do not

407   reflect CL seasons, which tends to indicate that this specimen lived in a less stable

408   environment than specimens US547-1 and US654-1. In this specimen, salinity must have

409   varied throughout the organism's lifespan, and probably from one season to the next (see

410   Fig. 4), suggesting some freshwater influence in substantial proportions to significantly

411   change the $\delta^{18}O_w$. Indeed, seasonal or monthly fluctuations in $\delta^{18}O_w$ have been reported to

412   induce errors of ± 3°C in estimations of sea surface temperatures compared to a mean

413   annual value, even without important freshwater influence (e.g. Prendergast et al., 2013).

414   For all specimens, none of the hypotheses (Atlantic Ocean or a Mediterranean Sea origin for

415   the oyster shells) can be ruled out from the reconstructed temperatures. As stable isotope

416   values cannot efficiently discriminate the living environment, other methods need to be

417   investigated.

418   <u>Environmental interpretation and collection sites in ancient times</u>

419   In view of the stable isotope data discussed above, we note an influence of the level of

420   freshwater input from rivers on Mg/Ca in addition to temperature. However, salinity was

421   reported to have no influence in Mg/Ca in mussel (Vander Putten et al., 2000) and oyster

422   shells (Mouchi et al., 2013; Surge and Lohmann, 2008; Tynan et al., *in press*) and Mg

423   concentrations in seawater is not linked to Mg incorporation in the shell (Tynan et al., *in*

424   *press*; Vander Putten et al., 2000). Given that alternative explanations for Mg/Ca variations

425   are not currently viable, the mean Mg/Ca content in oyster shells can be used to

426   characterize the living sites of specimens of unknown origin. Indeed, Bougeois et al. (2014,

427   2016) tested a variety of models on Eocene oyster shells from the Proto-Paratethys

428   epicontinental sea and the best fitting model for their shells corresponded to a model

429   defined with no direct influence of freshwater. We propose to use such an empirical

430   relationship to identify the environment of collection sites visited by fishermen during

431   Antiquity. The specific use for these models is practical here as the shells used in this study

432   were unearthed from a locality different to that of the (unknown) living environment of the

433   oysters.

434   A variety of shell Mg/Ca range values have been reported in the literature for normal

435   seawater temperature settings (Fig. 7). The differences transcribed in these relationships

436   probably represent several forcing factors of Mg incorporation.

437   Firstly, contrary to $\delta^{18}O$ that is in equilibrium with seawater for most molluscs and

438   foraminifera (Epstein et al., 1953; Erez and Luz, 1983), taxonomy has been suggested to have

439   an impact on Mg incorporation (Elderfield et al., 1996) but it appears not to be the case for

440   mussels and oysters, as indicated by the similar relationships (Fig. 7) found by Vander Putten

441   et al. (2000; *M. edulis*), Surge and Lohmann (2008; *C. virginica*) and Tynan et al. (*in press*;

442   *Saccostrea glomerata*). Moreover, similar Mg/Ca ranges were measured from specimens of

443   two oyster species (*O. edulis* and *C. gigas*) bred simultaneously on the same site (Mouchi et

444   al., 2013).

445   Shell Mg/Ca range is similar in the specimens bred in the same location (Mouchi et al., 2013;

446   Surge and Lohmann, 2008; Vander Putter et al., 2000; Tynan et al., *in press*), indicating that

447   the range of incorporation of Mg in bivalve shells depends much more on the locality and

448   the type of hydrologic settings than on potential vital effects. Indeed, shells from all

449   estuarine locations exhibit a strong Mg incorporation (Klein et al., 1996; Surge and Lohmann,

450   2008; Tynan et al., *in press*; Vander Putter et al., 2000), while all but one marine location

451   from those studied correspond to a weak Mg incorporation in bivalve shells. The location

452   that do not fit this observed relationship, Moreton Bay (Tynan et al., *in press*), presents a

453   typical marine salinity (35.1-36.7 ‰) but corresponds to a sheltered area with a relatively

454   long residence time of seawater (up to 100 days). This may be responsible for the

455   differences observed in Mg incorporation in bivalve shells compared to other sites with

456   more open marine influence.

457   The equation derived by Wanamaker et al. (2008) for *M. edulis* indicates high values of shell

458   Mg/Ca compared to other studies for similar temperatures. This model was established from

459   a laboratory experiment using water derived from seawater collected in the Damariscotta

460   River, Maine, far from the open sea. At this location, salinity is known to fluctuate from

461   season to season between 5 to 28 ‰ (Thompson et al., 2006), suggesting strong freshwater

462   input from rivers. The *M. edulis* models providing equivalent temperature values were

463   defined from locations presenting both open marine influence and freshwater input (Klein et

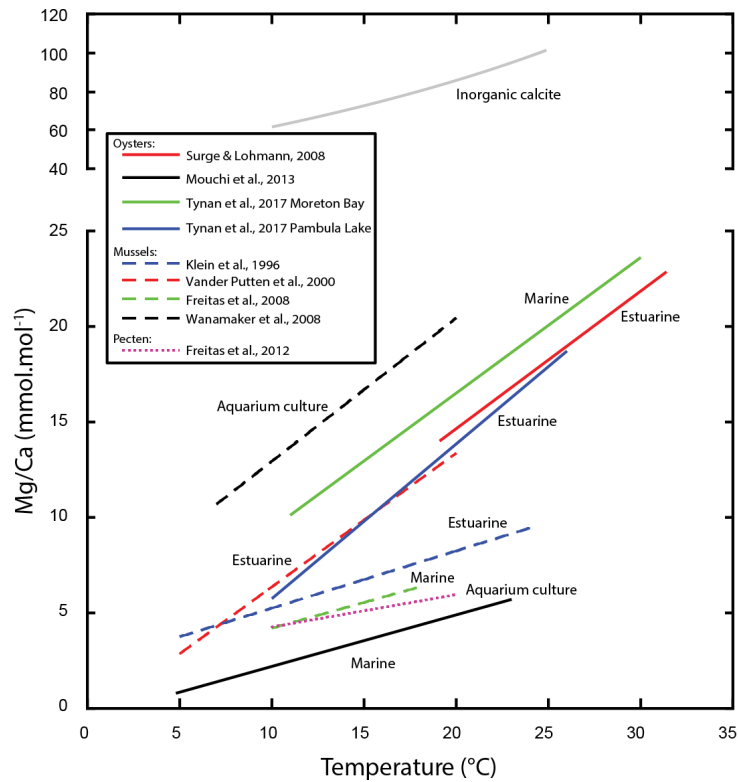464   al., 1996; Freitas et al., 2008).

465

466

Figure 7: Bivalve shell Mg/Ca range values for common seawater temperature settings from various published studies. Each relationship has been established from a different locality. Solid lines correspond to relationships measured from oysters, dashed lines correspond to the *Mytilus* mussel genus and the dotted line corresponds to *Pecten maximus*. Relationship for inorganic calcite is given for comparison.

The six specimens from our study can be associated with the environmental relationships of these models and by extension to the type of settings according to their Mg/Ca range values. In particular, specimens US547-1, US654-1 and US654-3 probably lived at locations subject to both marine and freshwater influence (Mg/Ca range: approx. 3-12 mmol.mol^{-1}). Interestingly, the age model from CL fluctuations indicates that the higher Mg/Ca values in specimen US654-1 occur during the winter months and the lower values during the summer months, as confirmed by temperatures calculated from δ^{18}O from this specimen. Such an

480 relationship between seasonal growth / temperature and Mn incorporation indicates that

481 Mn (as a CL activator) in this specimen is seasonally opposed to that of the other specimens

482 from this study and all modern specimens studied by Lartaud et al. (2010c) and Mouchi et al.

483 (2013). Such a difference may be caused by differences in seawater chemistry between the

484 living locality of US654-1 when compared to localities with no important freshwater input.

485 Additional examination under CL of other modern oyster shells from confirmed estuarine

486 areas would be required to check this assumption. Therefore, the locations of origin of

487 specimens US547-1, US654-1 and US654-3 may correspond to lagoons with partial

488 freshwater input from small rivers or groundwater.

489 Specimens US118-3 and US915-1, with low Mg/Ca values (approx. 0-5 mmol.mol^{-1}), are

490 generally compatible with an open marine environment. Specimen US118-3 presents the

491 particularity to change the amplitude of Mg/Ca values from simple to double around 5 mm

492 from the start of the umbo (after the second year of growth, according to the CL seasonal

493 calibration). This can be interpreted as a change in local hydrologic regime during the

494 organism lifespan, corresponding to an increased freshwater input. Growth rates (based on

495 CL seasonal calibration; Fig. 2) are indeed different for this specimen compared to the

496 others, as the shell appears to have grown faster during its fourth and seventh year and

497 slower the other years, suggesting an instable site in terms of food supply and favourable

498 environmental factors.

499 Finally, the Mg/Ca range in specimen US46-2 (approx. 10-30 mmol.mol^{-1}) indicates a strong

500 freshwater influence. As $\delta^{18}O$ values also reflect strong impact of freshwater input, the living

501 locality of this specimen must have been close to a river outlet.

502 The French Mediterranean coastline comprises numerous lagoons (Derolez et al., 2015) that

503 are partly supplied by freshwater from rivers and karstic groundwaters (Fleury et al., 2007).

504 Groundwater can have a strong influence on the water composition of lagoons and

505 substantially change water chemistry compared to adjacent areas (Stieglitz et al., 2013).

506 Therefore, the heterogeneity of geochemical signals in the oyster shells presented here

507 reflects a diversity of locality settings, most likely on the Mediterranean coastline.

508 The precise identification of the localities from which originated the oysters is impossible

509 with the present data and would require substantial analyses of the geochemistry of

510 multiple oyster shells from a variety of areas on the French Mediterranean coastline to be

511 compared with that of these specimens (although it cannot currently be excluded that these

512 specimens originated from other regions than the Mediterranean coastline). However, it

513 appears clear that specimen US46-2 originated from a different type of environment than

514 the other specimens. The locality for this specimen was subjected to an alternating and

515 strong freshwater influence, as suggested by the δ^{13}C and δ^{18}O data (Fig. 5). The largest

516 freshwater source in this region of the Mediterranean is the Rhone River. The Rhone River

517 forms a delta, hence providing an important flow of freshwater and large floods which could

518 possibly correspond to the results of δ^{18}O and mean Mg/Ca from this specimen.

519 However, the Rhone River may not have been the origin of specimen US46-2 as this outlet

520 (whose limits strongly varied over the ages) is too dynamic and unstable to grant survival of

521 long term oyster communities. Specimen US46-2 may have been collected from a large

522 estuary, close to the river outlet. An exact location for oyster harvest is however impossible

523 to determine at this time, partly due to the current complex coastline with multiple lagoons,

524 and partly because the position of the shoreline has changed since Antiquity (Bardot-Cambot

525 and Forest, 2015; Rey et al., 2005) and most lagoons are nowadays entirely emerged.

526 **Conclusion**

527 This study used two geochemical proxies for environmental reconstruction and

528 cathodoluminescence from six oyster shells on archaeological specimens dated from the 3rd

529 century AD to the 5th century AD and found in archaeological sites in Lyon, Central France.

530 Though the original living locality of these specimens is not known, the geochemical

531 heterogeneity among the shells indicates that these specimens did not live in the same area

532 and were under the influence of different mixing waters. Stable isotope analyses from three

533 shells indicate various regimes in freshwater input, with one specimen probably originating

534 from a locality in direct proximity to a river outlet while the two others present more stable

535 marine conditions.

536 As Mg/Ca ratio amplitude in bivalve shells has been reported to be different according to the

537 locality and the hydrologic setting in equivalent temperature ranges, we suggest that the

538 geochemical differences observed in each shell can be used to identify the environment

539 (estuary, lagoon, marine) from which the specimens originated. Our results indicate that

540 fishermen were probably not restricted to a single locality for oyster collection during

541 Antiquity but harvested oysters from a variety of areas. This study also highlights the

542 importance of careful choice of a Mg/Ca model to estimate palaeotemperatures in coastal

543 areas where freshwater input may have been a factor.

544

551

References

Anderson, T.F., Arthur, M.A., 1983. Stable isotopes of oxygen and carbon and their application to sedimentologic and paleoenvironmental problems. *In*: Arthur, M.A., Anderson, T.F., Kaplan, I.R., Veizer, J., Land, L. (Eds.), Stable isotopes in sedimentary geology, S.E.P.M., Short Course, 1-151.

Bardot-Cambot, A., 2014. Consommer dans les campagnes de la Gaule Romaine. *Revue du Nord*, Hors-série, Collection Art et Archéologie, 21, 109-123.

Bardot-Cambot, A., Forest, V., 2013. Ostréiculture et mytiliculture à l'époque romaine ? Des définitions modernes à l'épreuve de l'archéologie. *Revue archéologique*, 2013 fascicule 2, 367-388.

Bardot-Cambot, A., Forest, V., 2015. Du conchylioreste à l'environnement : de la nature à l'homme, de l'homme à la nature. *In*: Bardot-Cambot, A., Trannoy, L. (Eds.), L'environnement en mémoire, Presses universitaires de Rennes, ISBN 978-2-7535-4050-7, 11-24.

Bertrand, E., 2011. 16, rue Bourgelat – 69002 Lyon. Institut Saint-Vincent-de-Paul. Rapport de fouille d'archéologie préventive, Service archéologique de la ville de Lyon, 508 p.

Bougeois, L., de Rafélis, M., Reichart, G.-J., de Nooijer, L.J., Nicollin, F., Dupond-Nivet, G., 2014. A high resolution study of trace elements and stable isotopes in oyster shells to estimate Central Asian Middle Eocene seasonality. *Chemical Geology*, 363, 200-212.

Bougeois, L., de Rafélis, M., Reichart, G.-J., de Nooijer, L.J., Dupond-Nivet, G., 2016. Mg/Ca in fossil oyster shells as palaeotemperature proxy, an example from the Palaeogene of Central Asia. *Palaeogeography, Palaeoclimatology, Palaeoecology*, 441, 611-626.

Carozza, J.-M., Puig, C., Valette, P., Odiot, T., 2010. La plaine du Roussillon au cours de l'Holocène : apport d'une démarche géoarchéologique et géomorphologique à la connaissance des interactions homme-milieu. *Archéologie des rivages méditerranéens : 50*

576 *ans de recherche*, Errance, 37-46.

577 Carré, M., Bentaleb, I., Bruguier, O., Ordinola, E., Barrett, N.T., Fontugne, M., 2006.

578 Calcification rate influence on trace element concentrations in aragonitic bivalve shells:

579 evidences and mechanisms. *Geochimica et Cosmochimica Acta*, 70, 19, 4906–4920.

580 Craig, H., 1965. Measurements of oxygen isotope paleotemperatures. *In*: Tongiorgi, E. (Ed.),

581 Stable Isotopes in Oceanographic Studies and Paleotemperatures, ConsiglioNazionale Delle

582 Ricerche Laboratorio Di Geologia Nucleare, 161-182.

583 de Rafélis, M., Renard, M., Emmanuel, L., Durlet, C., 2000. Apport de la

584 cathodoluminescence à la connaissance de la spéciation du manganèse dans les carbonates

585 pélagiques. *Comptes Rendus de l'Académie des Sciences - Series IIA - Earth and Planetary*

586 *Science*, 330, 391-398.

587 Derolez, V., Oheix, J., Ouisse, V., Munaron, D., Fiandrino, A., Messiaen, G., Hubert, C.,

588 Lamoureux, A., Malet, N., Fortune, M., Berard, L., Mortreux, S., Guillou, J.-L., 2015. Suivi

589 estival des lagunes méditerranéennes françaises - Bilan des résultats 2014. IFREMER

590 publication http://archimer.ifremer.fr/doc/00273/38461/.

591 Dubar, M., 2003. The Holocene deltas of Eastern Provence and the French Riviera:

592 geomorphological inheritance, genesis and vulnerability. *Geomorphologie : relief, processus,*

593 *environnement*, 4, 263-270.

594 Duprey, N., Lazareth, C.E., Dupouy, C., Butscher, J., Farman, R., Maes, C., Cabioch, G., 2015.

595 Calibration of seawater temperature and $\delta^{18}O$seawater signals in Tridacna maxima's

596 $\delta^{18}O$shell record based on in situ data. *Coral Reefs*, 34, 437-450.

597 Elderfield, H., Bertram, C.J., Erez, J., 1996. A biomineralization model for the incorporation of

598 trace elements into foraminiferal calcium carbonate. *Earth and Planetary Science Letters*,

599 142, 409-423.

600   Emery, K.A., Wilkinson, G.M., Camacho-Ibar, V.F., Pace, M.L., McGlathery, K.J., Sandoval-Gil,

601   J.M., Hernandez-Lopez, J., 2016. Resource use of an aquacultured oyster (*Crassostrea gigas*)

602   in the reverse estuary Bahia San Quintin, Baja California, Mexico. *Estuaries and Coasts*, 39,

603   866-874.

604   Epstein, S., Mayeda, T., 1953. Variation of O^{18} content of waters from natural sources.

605   *Geochimica et Cosmochimica Acta*, 4, 213-224.

606   Epstein, S., Buchsbaum, R., Lowenstam, H.A., Urey, H.C., 1951. Carbonate-water isotopic

607   temperature scale. *Bulletin of the Geological Society of America*, 62, 417-426.

608   Epstein, S., Buchsbaum, R., Lowenstam, H.A., Urey, H.C., 1953. Revised carbonate-water

609   isotopic temperature scale. *Bulletin of the Geological Society of America*, 64, 1315-1326.

610   Erez, J., Luz, B., 1983. Experimental paleotemperature equation for planktonic foraminifera.

611   *Geochimica et Cosmochimica Acta*, 47, 1025-1031.

612   Faget D., 2007. Cultiver la mer : biodiversité marine et développement de l'ostréiculture

613   dans le Midi méditerranéen français au XIXe siècle. *In*: Annales du Midi : revue

614   archéologique, historique et philologique de la France méridionale, Tome 119, 258. Les

615   triens mérovingiens en Limousin, 207-226, doi : 10.3406/anami.2007.7177.

616   Fleury, P., Bakalowicz, M., de Marsily, G., 2007. Submarine springs and coastal karst aquifers:

617   A review. *Journal of Hydrology*, 339, 79-92.

618   Freitas, P., Clarke, L., Kennedy, H., Richardson, C., 2008. Inter-and intra-specimen variability

619   masks reliable temperature control on shell Mg/Ca ratios in laboratory and field cultured

620   *Mytilus edulis* and *Pecten maximus* (Bivalvia). *Biogeoscience Discussions*, 5.

621   Freitas, P.S., Clarke, L.J., Kennedy, H., Richardson, C.A., 2012. The potential of combined

622   Mg/Ca and $\delta^{18}O$ measurements within the shell of the bivalve *Pecten maximus* to estimate

623   seawater $\delta^{18}O$ composition. *Chemical Geology*, 291, 286-293.

624   Gaudron, S.M., Grangeré, K., Lefebvre, S., 2016. The comparison of $\delta^{13}C$ values of a deposit-

625   and a suspension-feeder bio-indicates benthic vs. pelagic couplings and trophic status in

626   contrasted coastal ecosystems. *Estuaries and Coasts*, 39, 731-741.

627   Gillikin, D.P., Lorrain, A., Navez, J., Taylor, J.W., André, L., Keppens, E., Baeyens, W., Dehairs,

628   F., 2005. Strong biological controls on Sr /Ca ratios in aragonitic marine bivalve shells.

629   *Geochemistry, Geophysics, Geosystems*, 6, 5, doi:10.1029/2004GC000874.

630   Hofmann, E., in prep. Fouille de l'îlot central de l'Antiquaille (Lyon, 5e arrondissement).

631   Rapport de fouilles.

632   Kirby, M.X., Soniat, T.M., Spero, H.J., 1998. Stable isotope sclerochronology of Pleistocene

633   and Recent oyster shells (*Crassostrea virginica*). *Palaios*, 13, 560-569.

634   Klein, R.T., Lohmann, K.C., Thayer, C.W., 1996. Bivalve skeletons record seas-surface

635   temperature and $\delta^{18}O$ via Mg/Ca and $^{18}O/^{16}O$ ratios. *Geology*, 24, 415-418.

636   Langlet, D., Alunno-Bruscia, M., de Rafélis, M., Renard, M., Roux, M., Schein, E., Buestel, D.,

637   2006. Experimental and natural cathodoluminescence in the shell of *Crassostrea gigas* from

638   Thau lagoon (France): ecological and environmental implications. *Marine Ecology Progress*

639   *Series*, 317, 143-156.

640   Lartaud, F., 2007. Les fluctuations haute fréquence de l'environnement au cours des temps

641   géologiques. Mise au point d'un modèle de référence actuel sur l'enregistrement des

642   contrastes saisonniers dans l'Atlantique nord. Ph.D thesis, UPMC-Paris 06, 336 p.

643   Lartaud, F., Langlet, D., de Rafélis, M., Emmanuel, L., Renard, M., 2006. Description of

644   seasonal rythmicity in fossil oyster shells *Crassostrea aginensis* Tournouer, 1917 (Aquitanian)

645   and *Ostrea bellovacina* Lamarck, 1806 (Thanetian). Cathodoluminescence and

646   sclerochronological approaches. *Geobios*, 39, 845-852. doi:10.1016/j.geobios.2005.11.001.

647   Lartaud, F., Emmanuel, L., de Rafélis, M., Ropert, M., Labourdette, N., Richardson, C.A.,

648   Renard, M., 2010a. A latitudinal gradient of seasonal temperature variation recorded in

649   oyster shells from the coastal waters of France and The Netherlands. *Facies*, 56, 13-25.

650   Lartaud, F., Emmanuel, L., De Rafelis, M., Pouvreau, S., Renard,M., 2010b. Influence of food

651   supply on the δ^{13}C signature of mollusc shells: implications for palaeoenvironmental

652   reconstitutions. *Geo-Marine Letters*, 30, 23-34.

653   Lartaud, F., de Rafélis, M., Ropert, M., Emmanuel, L., Geairon, P., Renard, M., 2010c. Mn

654   labelling of living oysters: Artificial and natural cathodoluminescence analyses as a tool for

655   age and growth rate determination of *C. gigas* (Thunberg, 1793) shells. *Aquaculture*, 300,

656   206-217.

657   Lazareth, C.E., Vander Putten, E., André, L., Dehairs, F., 2003. High-resolution trace element

658   profiles in shells of the mangrove bivalve *Isognomon ephippium*: a record of environmental

659   spatio-temporal variations? *Estuarine, Coastal and Shelf Science*, 57, 1103-1114.

660   Lorrain, A., Gillikin, D., Paulet, Y.-M., Chauvaud, L., Le Mercier, A., Navez, J., André, L., 2005.

661   Strong kinetic effects on Sr/Ca ratios in the calcitic bivalve *Pecten maximus*. *Geology*, 33, 12,

662   965-968.

663   Luterbacher, J., Werner, J.-P., Smerdon, J.-E., Fernandez-Donado, L., Gonzales-Rouco, J.-F.,

664   Barriopedro, D., Ljungqvist, F.-C., Buntgen, U., Zorita, E., 2016. European summer

665   temperatures since Roman Times. *Environmental Research Letters*, 11, 024001.

666   McCrea, J.M., 1950. On the isotopic chemistry of carbonates and a paleotemperature scale.

667   *The Journal of Chemical Physics*, 18, 849-857.

668   McConnaughey, T.A., Gillikin, D.P., 2008. Carbon isotopes in mollusk shell carbonates. *Geo-

669   Marine Letters*, 28, 287-299. doi: 10.1007/s00367-008-0116-4.

670   Mouchi, V., de Rafélis, M., Lartaud, F., Fialin, M., Verrecchia, E., 2013. Chemical labelling of

671   oyster shells used for time-calibrated high-resolution Mg/Ca ratios: A tool for estimation of

672   past seasonal temperature variations. *Palaeogeography, Palaeoclimatology, Palaeoecology*,

673   373, 66-74.

674   Pierre, C., 1999. The oxygen and carbon isotope distribution in the Mediterranean water

675   masses. *Marine Geology*, 153, 41-55.

676   Poulain, C., Gillikin, D.P., Thébault, J., Munaron, J.M., Bohn, M., Robert, R., Paulet, Y.-M.,

677   Lorrain, A., 2015. An evaluation of Mg/Ca, Sr/Ca, and Ba/Ca ratios as environmental proxies

678   in aragonite bivalve shells. *Chemical Geology*, 396, 42-50.

679   Prendergast, A.L., Azzopardi, M., O'Connell, T.C., Hunt, C., Barker, G., Stevens, R.E., 2013.

680   Oxygen isotopes from *Phorcus (Osilinus) turbinatus* shells as a proxy for sea surface

681   temperature in the central Mediterranean: A case study from Malta. *Chemical Geology*, 345,

682   77-86.

683   Raynal, O., Bouchette, F., Certain, R., Séranne, M., Sabatier, P., Lofi, J., Dezileau, L., Briquieu,

684   L., Pezard, P., Courp, P., 2010. Holocene evolution of languedocian lagoonal environment

685   controlled by inherited coastal morphology (northern Gulf of Lions, France). *Bulletin de la*

686   *Société Géologique de France*, 181, 2, 211-224.

687   Rescanières, S., 2002. Essai sur le cadre géographique antique du Narbonnais. *In* : Dellong E.

688   (Ed.), Narbonne et le Narbonnais (11/1), Carte archéologique de la Gaule, Paris, France, 44-

689   51.

690   Rey, T., Lefevre, D., Vella, C., 2005. Données nouvelles sur les lobes deltaïques du paléogolf

691   d'Aigues-Mortes à l'Holocène [Petite Camargue, France]. *Quaternaire*, 16, 329-338.

692   Rey, T., Lefevre, D., Vella C., 2009. Deltaic plain development and environmental changes in

693   the Petite Camargue, Rhône Delta, France, in the past 2000 years. *Quaternary Research*, 71,

694   284-294.

695   Richardson, C., Collis, S., Ekaratne, K., Dare, P., Key, D., 1993. The age determination and

696   growth rate of the European flat oyster, *Ostrea edulis*, in British waters determined from

697   acetate peels of umbo growth lines. *ICES Journal of Marine Science*, 50, 493-500.

698   Rohling, E.J., 2000. Paleosalinity: confidence limits and future applications. *Marine Geology*,

699   163, 1-11.

700   Saenger, C., Wang, Z., 2014. Magnesium isotope fractionation in biogenic and abiogenic

701   carbonates: implications for paleoenvironemental proxies. *Quaternary Science Reviews*, 90,

702   1-21.

703   Schöne, B.R., Gillikin, D.P., 2013. Unraveling environmental histories from skeletal diaries —

704   Advances in sclerochronology. *Palaeogeography, Palaeoclimatology, Palaeoecology*, 373, 1-

705   5.

706   Stenzel, H.B., 1971. Oysters. *Treatise on Invertebrate Paleontology*, 3, 953-1184.

707   Stieglitz, T., van Beek, P., Souhaut, M., Cook, P.G., 2013. Karstic groundwater discharge and

708   seawater recirculation through sediments in shallow coastal Mediterranean lagoons,

709   determined from water, salt and radon budgets. *Marine Chemistry*, 156, 73-84.

710   Sunda, W.G., Huntsman, S.A., 1985. Regulation of cellular manganese and manganese

711   transport rates in the unicellular alga *Chlamydomonas*. *Limnology and Oceanography*, 30,

712   567-586.

713   Surge, D., Walker, K.J., 2006. Geochemical variation in microstructural shell layers of the

714   southern quahog (*Mercenaria campechiensis*): Implications for reconstructing seasonality.

715   *Palaeogeography, Palaeoclimatology, Palaeoecology*, 237, 182-190.

716   Surge, D., Lohmann, K.-C., 2008. Evaluating Mg/Ca ratios as a temperature proxy in the

717   estuarine oyster, *Crassostrea virginica*. *Journal of Geophysical Research*, 113, G02001.

718   Surge, D.M., Lohmann, K.C., Dettman, D. L., 2001. Controls on isotopic chemistry of the

719   American oyster, *Crassostrea virginica*: Implications for growth patterns. *Palaeogeography,*

720   *Palaeoclimatology, Palaeoecology*, 172, 283-296.

721   Surge, D., Lohmann, K.C., Goodfriend, G.A., 2003. Reconstructing estuarine conditions:

722   Oyster shells as recorders of environmental change, southwest Florida. *Estuarine, Coastal*

723   *and Shelf Science*, 57, 737-756.

724   Thompson, B., Perry, M.J., Davis, C., 2006. Phytoplankton in the Damariscotta River Estuary.

725   *Marine Research in focus*, Sept. 2006, 3, 4 p.

726   Tynan, S., Opdyke, B.N., Walczak, M., Eggins, S., Dutton, A., in press. Assessment of Mg/Ca in

727   *Saccostrea glomerata* (the Sydney rock oyster) shell as a potential temperature record.

728   *Palaeogeography, Palaeoclimatology, Palaeoecology*,

729   http://dx.doi.org/10.1016/j.palaeo.2016.08.009.

730   Ullmann, C.V., Böhm, F., Rickaby, R.E.M., Wiechert, U., Korte, C., 2013. The Giant Pacific

731   Oyster (*Crassostrea gigas*) as a modern analog for fossil ostreoids: Isotopic (Ca, O, C) and

732   elemental (Mg/Ca, Sr/Ca, Mn/Ca) proxies. *Geochemistry, Geophysics, Geosystems*, 14, 4109-

733   4120, doi:10.1002/ggge.20257.

734   Urey, H.C., Lowenstam, H.A., Epstein, S., McKinney, C.R., 1951. Measurement of

735   paleotemperatures and temperatures of the Upper Cretaceous of England, Denmark, and

736   the Southeastern United States. *Bulletin of the Geological Society of America*, 62, 399-416.

737   Vander Putten, E., Dehairs, F., Keppens, E., Baeyens, W., 2000. High resolution distribution of

738   trace elements in the calcite shell layer of modern *Mytilus edulis*: environmental and

739   biological controls. *Geochimica et Cosmochimica Acta*, 64, 997-1011.

740   Voelker, A.H.L., Colman, A., Olack, G., Waniek, J.J., Hodell, D., 2015. Oxygen and hydrogen

741   isotope signatures of Northeast Atlantic water masses. *Deep-Sea Research II*, 116, 89-106.

742   Wanamaker, A.D., Kreutz, K.J., Wilson, T., Borns Jr., H.W., Introne, D.S., Feindel, S., 2008.

743   Experimentally determined Mg/Ca and Sr/Ca ratios in juvenile bivalve calcite for *Mytilus*

744   *edulis*: implications for paleotemperature reconstructions. *Geo-Marine Letters*, 28, 359-368.

745   Walther, B.D., Rowley, J.L., 2013. Drought and flood signals in subtropical estuaries recorded

746   by stable isotope ratios in bivalve shells. *Estuarine, Coastal and Shelf Science*, 133, 235-243.

747

748   SUPPLEMENTARY INFORMATION

749

750   Table 1: Thermodependance equations of Mg/Ca in mollusc shells from breeding experiments
751   according to the type of locality.

752

ENVIRONMENT	SPECIES	EQUATION	REFERENCE
ESTUARINE	*Crassostrea virginica*	Mg/Ca = 0.72*T +0.25	Surge and Lohmann (2008)
	Mytilus edulis	Mg/Ca = 0.70*T – 0.63	Vander Putten et al. (2000)
	Mytilus trossulus	Mg/Ca = 0.30*T + 2.25	Klein et al. (1996)
	Saccostrea glomerata	Mg/Ca = 0.81*T – 2.35	Tynan et al. (2016)
OPEN MARINE	*Crassostrea gigas*	Mg/Ca = 0.27*T – 0.5	Mouchi et al. (2013)
	Mytilus edulis	Mg/Ca = 0.27*T + 1.5	Freitas et al. (2008)
	Saccostrea glomerata	Mg/Ca = 0.71*T + 2.31	Tynan et al. (2016)
AQUARIUM	*Mytilus edulis*	Mg/Ca = 0.75*T +5.44	Wanamaker et al. (2008)
	Pecten maximus	Mg/Ca = 0.17*T + 2.56	Freitas et al. (2012)

753